Physical properties of sprayed antimony doped tin oxide thin films: The role of thickness

A. R. Babar[1], S. S. Shinde[1], A.V. Moholkar[1], C. H. Bhosale[1], J. H. Kim[2], and K. Y. Rajpure[1,†]

[1]Electrochemical Materials Laboratory, Department of Physics, Shivaji University, Kolhapur-416 004, India
[2]Department of Materials Science and Engineering, Chonnam National University, 300 Yongbong-Dong, Buk-Gu, Gwangju, 500-757, South Korea

Abstract: Transparent conducting antimony doped tin oxide ($Sb:SnO_2$) thin films have been deposited onto pre-heated glass substrates using a spray pyrolysis technique by varying the quantity of spraying solution. The structural, morphological, X-ray photoelectron spectroscopy, optical, photoluminescence and electrical properties of these films have been studied. It is found that the films are polycrystalline in nature with a tetragonal crystal structure having orientation along the (211) and (112) planes. Polyhedrons like grains appear in the FE-SEM images. The average grain size increases with increasing spraying quantity. The compositional analysis and electronic behaviour of $Sb:SnO_2$ thin films were studied using X-ray photoelectron spectroscopy. The binding energy of $Sn3d_{5/2}$ for all samples shows the Sn^{4+} bonding state from SnO_2. An intensive violet luminescence peak near 395 nm is observed at room temperature due to oxygen vacancies or donor levels formed by Sb^{5+} ions. The film deposited with 20 cc solution shows 70 % transmittance at 550 nm leading to the highest figure of merit ($2.11 \times 10^{-3}\ \Omega^{-1}$). The resistivity and carrier concentration vary over 1.22×10^{-3} to $0.89 \times 10^{-3}\ \Omega$·cm and 5.19×10^{20} to $8.52 \times 10^{20}\ cm^{-3}$, respectively.

Key words: semiconductors; microstructure; optical properties; electrical properties
DOI: 10.1088/1674-4926/32/5/053001 **EEACC:** 2520

1. Introduction

Electrically conductive materials with high optical transmittance are key elements for thin film solar cells and display devices. Amongst them, transparent conductive oxides (TCO), based on high band gap, degenerate semiconductors are mechanically hard and can withstand high temperatures. Along with this, wide and direct band gap semiconductor materials are of much interest for blue and ultraviolet (UV) optical devices, such as light-emitting diodes and laser diodes[1]. As wide band gap semiconductors, SnO_2 and doped SnO_2 are known to have a wide range of technological applications, such as transparent conducting electrodes, dye-sensitized solar cells[2,3] and chemical sensors[4,5], and now they seem to be more attractive for their luminescence properties[6–8]. Antimony doped tin oxide ($Sb:SnO_2$) thin films are deposited by various methods, viz. sputtering[9], chemical vapour deposition[10], DC glow discharge[11], dip coating[12], sol–gel[13] and spray pyrolysis[14–16]. Spray pyrolysis is a promising technique for producing sufficiently conductive and adherent $Sb:SnO_2$ thin films in a cost-effective way.

Kaneko *et al.*[17] investigated the physical properties of $Sb:SnO_2$ thick films (4000–14000 Å) deposited onto fused quartz, borosilicate and soda lime glasses. They showed that the electrical resistivity and optical band gap are independent of film thickness deposited on fused quartz and borosilicate. Ma *et al.*[18] reported the dependence of film thickness on the physical properties of SnO_2:Sb films deposited on flexible substrates by RF magnetron sputtering. They observed that mobility increases with thickness and resistivity decreases. Agashe *et al.*[19] studied the competitive effects of film thickness and growth rate in spray pyrolytically deposited fluorine-doped tin oxide films. The thickness evolution involved textured growth along the [200] orientation followed by a secondary prominence of [110] and [101] orientations. The growth rate induced effects accelerated this change. The carrier concentration and carrier mobility showed that the [200] oriented growth is technologically advantageous and can be obtained using a wider growth rate range of ~ 50–130 nm/min. Yannopoulos[20] studied the use of stannic oxide thick films that incorporate antimony as a structural dopant for sensing combustible gases in oxidizing and fixed water vapour-containing atmospheres.

In the present investigation, we have studied the effect of thickness on the physicochemical properties of $Sb:SnO_2$ thin films synthesized by spray pyrolysis. The growth mechanism has been correlated to use these films in gas sensor and optoelectronic devices.

2. Experimental

Stannic chloride (Thomas Baker) and antimony trichloride (s.d. fine), respectively, were used as precursors for tin and antimony. The glass substrates ($75 \times 25 \times 1.2\ mm^3$) supplied by Blue Star, Mumbai, were used. The required amount of $SbCl_3$ dissolved in 1M HCl was added to 2M aqueous $SnCl_4 \cdot 5H_2O$ solution to obtain 2 at% Sb doping in the starting solution[21]. This was taken as the stock solution. Ten millilitres of propan-2-ol was added to the ten millilitres of stock solution before spraying. The amount of $SbCl_3$ was kept fixed at 2 at% for antimony doping, which has been found to be optimal for good

† Corresponding author. Email: rajpure@yahoo.com
Received 25 October 2010, revised manuscript received 8 December 2010

Table 1. Various parameters estimated for sprayed Sb:SnO_2 thin films with various quantities of spraying solution (R_s = sheet resistance, ρ = resistivity, n = carrier concentration, μ = mobility, ϕ = figure of merit, E_f = Fermi energy, l = mean free path, t = thickness, CS = crystallite size, ω_p = plasma frequency, $\%T$ = transmittance of the films).

Spraying solution quantity (cc)	R_s (Ω)	ρ (10^{-3} Ω·cm)	N (10^{20} cm^{-3})	μ (cm^2/(V·s))	ϕ ($10^{-3}\Omega^{-1}$)	E_f (eV)	l (Å)	t (nm)	CS (nm)	ω_p (10^{15} Hz)	$\%T$ at $\lambda = 550$ nm
20	15.42	1.22	5.19	9.83	2.11	1.24	16.07	794	19.86	3.30	71
30	11.65	1.13	6.31	8.75	0.12	1.41	15.26	969	24.5	3.65	51
40	8.84	0.89	8.52	7.49	0.015	1.72	14.44	1104	27.56	4.24	41

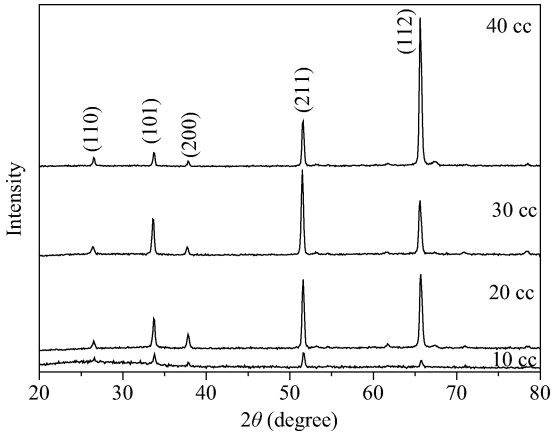

Fig. 1. XRD patterns of the Sb:SnO_2 thin films deposited for various amounts of spraying solution.

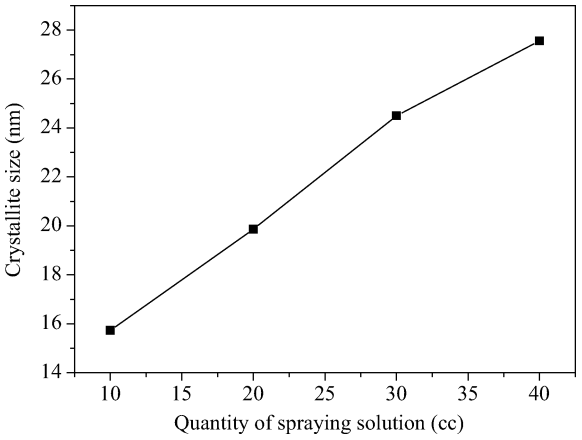

Fig. 2. Variation in average crystallite size of sprayed Sb:SnO_2 thin films for different quantities of spraying solution.

quality films obtained earlier. The quantity of spraying solution was varied from 10 to 40 cubic centimetres (cc). The substrates were maintained at 475 ℃ optimal temperature for formation of pyrolytically decomposed good quality Sb:SnO_2 films. These films were then allowed to cool at room temperature and further used for structural, optical, electrical characterizations etc. The structural properties were studied by a powder X-ray diffractometer (Bruker D8 Advance, France) using Cu-Kα radiation in the span of 20°–80°. The morphology of the films was observed by field emission scanning electron microscopy (FE-SEM, Model: JSM-6701F, Japan). XPS studies were carried out using model PHI-5400 type X-ray photoelectron spectroscopy (XPS, physical electronics PHI 5400, USA) with a monochromatic Mg-Kα (1254 eV) radiation source. An optical absorption study was carried out in the wavelength range of 200–1100 nm using a double beam spectrophotometer (SHIMADZU UV-1700, Japan). The electrical properties were studied by using a Hall effect setup (Scientific Instruments, DHE-21, India) in the Van der Pauw configuration.

3. Results and discussion

3.1. Structural analysis

Table 1 shows the variation in film thickness as a function of the quantity of spraying solution, from which it is seen that the film thickness increases with the quantity of spraying solution. The expected reason for this is the supply of more ingredient ions with an increasing quantity of spraying solution. The XRD patterns for the Sb:SnO_2 thin films grown on glass substrates were studied in the 2θ range of 20°–80° shown in Fig. 1. It is seen that the material deposited is polycrystalline irrespective of the quantity of spraying solution. The presence of a tetragonal crystal structure has been confirmed from matching of observed and standard d (inter planer spacing) values. No other extra phases (such as SnO, Sn_2O_3 and Sb_2O_3) are observed in the deposited thin films. It is found that the film tends to grow in specific (211) and (112) crystallographic directions. However, as the quantity of solution is increased, the intensity of the (211) peak decreases and the intensity of the (112) peak increases, indicating a slight crystal reorientation effect. The variation in preferred orientation with respect to the quantity of spraying solution may be attributed to the change in film thickness[22]. Above 40 cc, milky and powdery films resulted.

The crystallite size D is calculated using Scherrer's formula,

$$D = \frac{0.9\lambda}{\beta \cos\theta}, \tag{1}$$

where D is the crystallite size, β is the broadening of the diffraction line measured at half of its maximum intensity (rad.) FWHM and λ is the X-ray wavelength (1.5406 Å). The variation in average crystallite size with the quantity of spraying solution for Sb:SnO_2 thin films is shown in Fig. 2. It is seen that the crystallite size increases with an increase in spraying solution. The analysis reveals that the quantities of spraying solution strongly influence the crystallite size as well as the thickness of the thin films.

The reflection intensities from each XRD pattern contain information related to the preferential or random growth of

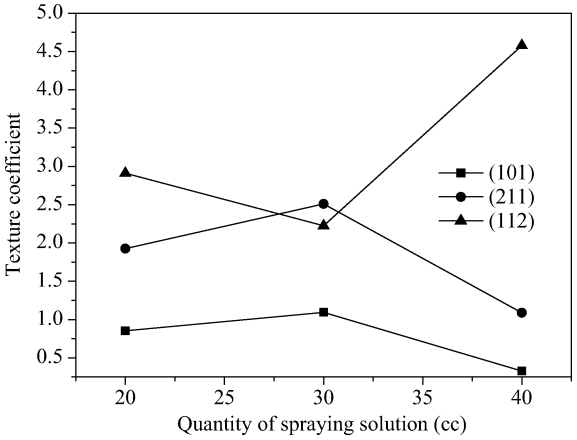

Fig. 3. Variation in TC (101), TC (211) and TC (112) of Sb:SnO_2 thin films for different quantities of spraying solution.

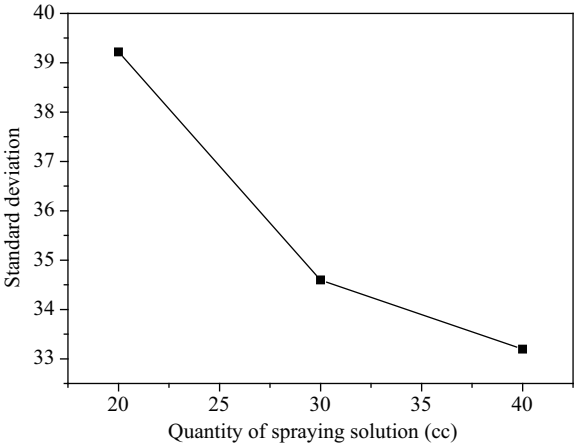

Fig. 4. Variation in standard deviation for quantities of spraying solution for Sb:SnO_2 thin films.

polycrystalline thin films, which is studied by calculating the texture coefficient $TC_{(hkl)}$ for all planes using[23]

$$TC_{(hkl)} = \frac{I_{(hkl)}/I_{0(hkl)}}{(1/N)\sum I_{(hkl)}/I_{0(hkl)}}, \quad (2)$$

where $I_{(hkl)}$ is the measured intensity of X-ray reflection, $I_{0(hkl)}$ is the corresponding standard intensity from the JCPDS data card No-01-0625 and N is the number of reflections observed in the XRD pattern. Figure 3 depicts the variation in the texture coefficient with the quantity of spraying solution for the (101), (211) and (112) planes. For 20 cc solution, $TC_{(112)}$ has a relatively higher value than the other planes (101) and (211). $TC_{(112)}$ slightly decreases for 30 cc and further increases for a higher solution quantity (40 cc). This confirms the crystal reorientation effect.

In order to understand the growth mechanism involved in spray deposited Sb:SnO_2 films at various quantities of spraying solution, the standard deviation (σ) was estimated by using the equation

$$\sigma = \sqrt{\frac{\sum I_{hkl}^2 - [(I_{hkl})^2/2]}{N}}, \quad (3)$$

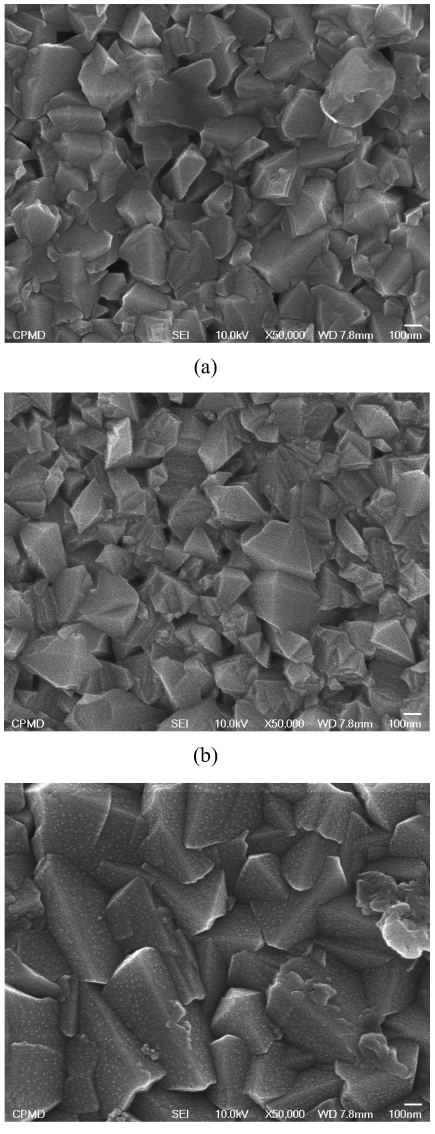

Fig. 5. FE-SEM micrographs of Sb:SnO_2 thin films prepared for (a) 20, (b) 30, (c) 40 cc spraying solution. Magnification: 20000 ×.

where I stands for the relative intensity of the (hkl) plane. The variation in standard deviation with the quantity of spraying solution is shown in Fig. 4. Initially at 20 cc, the nucleation and adsorption–desorption phenomenon seems to be predominant, as a result of heterogeneous nucleation resulting in relatively higher σ values. A decrease in σ values with further increase in spraying solution suggests the onset of homogeneous nucleation.

3.2. Morphological study

Figures 5(a)–5(c) show scanning electron micrographs (SEM) of Sb:SnO_2 films deposited on glass substrates. It is observed that the surface morphology of the films was strongly dependent upon the quantity of spraying solution. It is seen that the layers are made up of grains with polyhedron like shapes. The presence of big and faceting nanocrystals observed in these images present the fact that the polyhedron crystallites are formed by coalescence. The average grain size increases

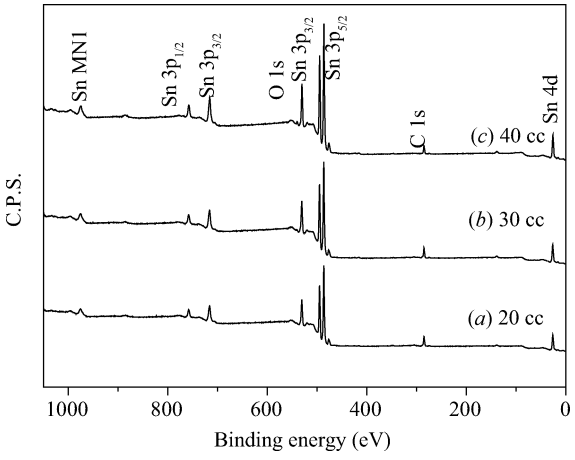

Fig. 6. XPS survey scan spectra of Sb:SnO_2 thin films deposited for different quantities of spraying solution. (*a*) 20 cc. (*b*) 30 cc. (*c*) 40 cc.

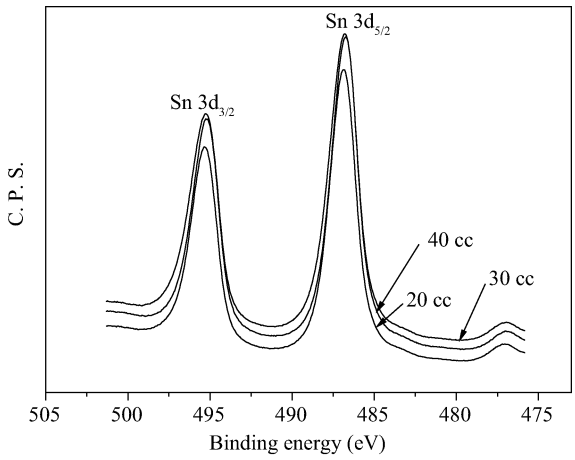

Fig. 7. Sn3d narrow scan XPS spectra of Sb:SnO_2 thin films deposited for various quantities of spraying solution.

with increasing spraying quantity. At 20 cc solution quantity, small polyhedrons like grains are observed. As the quantity increased further, the polyhedron-like grains dwindled and were hardly distinguished from the small grains. The grains are randomly grown giving rise to a scattering effect, thereby reducing transmittance.

3.3. X-ray photoelectron spectroscopy

Figure 6 shows the X-ray photoelectron spectroscopy (XPS) survey scan of thin films deposited with various solution quantities (20, 30, 40 cc). The sample contains Sn, Sb, O and traces of C having a SnMN1 auger peak with Sn3p, Sn3d, Sn4d core levels. The presence of a C1s peak in the spectra can be attributed to contamination which resulted from the samples being exposed to air before the XPS measurements[24].

Narrow scan XPS spectra of Sn3d state for the samples are shown in Fig. 7. The spectra show well-resolved doublets due to the $Sn3d_{5/2}$ and $3d_{3/2}$ components corresponding to binding energies of 486.86, 486.78, 486.73 eV and 495.29, 495.22, 495.19 eV for 20, 30, 40 cc, respectively. The binding energy of $Sn3d_{5/2}$ is attributed to the Sn^{4+} bonding state, which agrees

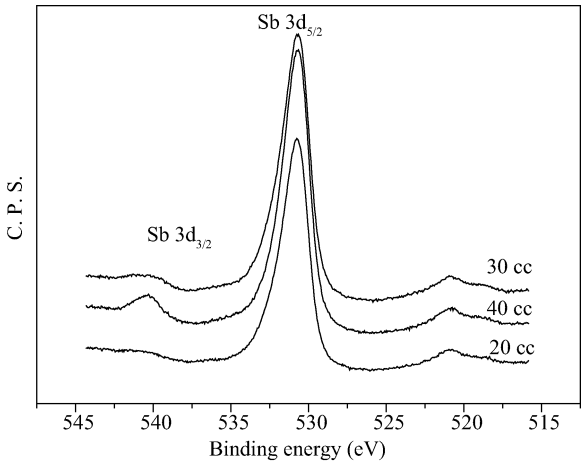

Fig. 8. Sb3d narrow scan XPS spectra of Sb:SnO_2 thin films deposited at various quantities of spraying solution.

well with the previous report[25]. The gap between the $Sn3d_{3/2}$ and $Sn3d_{5/2}$ levels ($\approx$ 8.45 eV) closely corresponds to the O in SnO_2 and Sn in SnO_2, respectively[26]. Figure 8 shows the narrow scan XPS spectra of Sb3d state for the samples deposited with various solution quantities. At a low doping concentration of Sb, we observe the lower intensity peak of the $Sb3d_{3/2}$ state. Terrier *et al.*[27] reported that the major Sb oxidation states existed for Sb^{5+} state at a lower doping level and a Sb^{3+} state at higher doping level. They showed that the Sb^{5+} and Sb^{3+}peak position was located at binding energies of 540.1 eV and 539.2 eV, respectively. In our study, all of the samples show the binding energy of $Sb3d_{5/2}$ (shown in Fig. 8) in the region of 530.6–530.9 eV, indicating that all antimony detected was in a pentavalent state (Sb^{5+})[28].

Narrow scan XPS spectra of the O1s state for samples deposited with various solution quantities (20–40 cc) are shown in Figs. 9(a)–9(c). Gaussian curve fitting illustrates that the O1s peak has a doublet component; such a phenomenon is common for oxides containing oxygen in multiple valence states[29]. The binding energies of O1s are 530.55, 532.02; 530.45, 531.72 and 530.57, 531.70 eV for 20, 30 and 40 cc, respectively. Generally, the O1s peak observed in the region 529–530 eV has been attributed to lattice oxygen. Ghuang *et al.*[30] attributed the peak around 530.7–531.6 eV to oxygen in non-stoichiometric oxides in the surface region. They observed chemisorbed O_2 on the metal surface in 530–530.9 eV and surface oxides and hydroxides in 529.6–531.0 eV and 533.3 eV binding energy regions, respectively. Sharma *et al.*[31] have assigned the 532 eV peak to absorbed hydroxyl ions. Srinivasan *et al.*[32] have attributed the peak at 531.7 eV to chemisorbed oxygen. On the basis of the above, the O1s peak observed in the region 530.45–530.57 eV for Sb:SnO_2 thin film prepared by spray pyrolysis in the present work can be attributed to chemisorbed oxygen. The peak appeared around 532 eV attributed to the OH group linked to Sn. This has been observed for all samples, indicating that the samples are hygroscopic in nature[33].

The ratio of atomic concentrations (O/Sn) is quantitatively analyzed by calculating the peak areas of the O1s and $Sn3d_{5/2}$ peaks. The obtained values are 1.86, 1.87, 2.01 for 20, 30, 40 cc, respectively. These values deviate from the theoretical one,

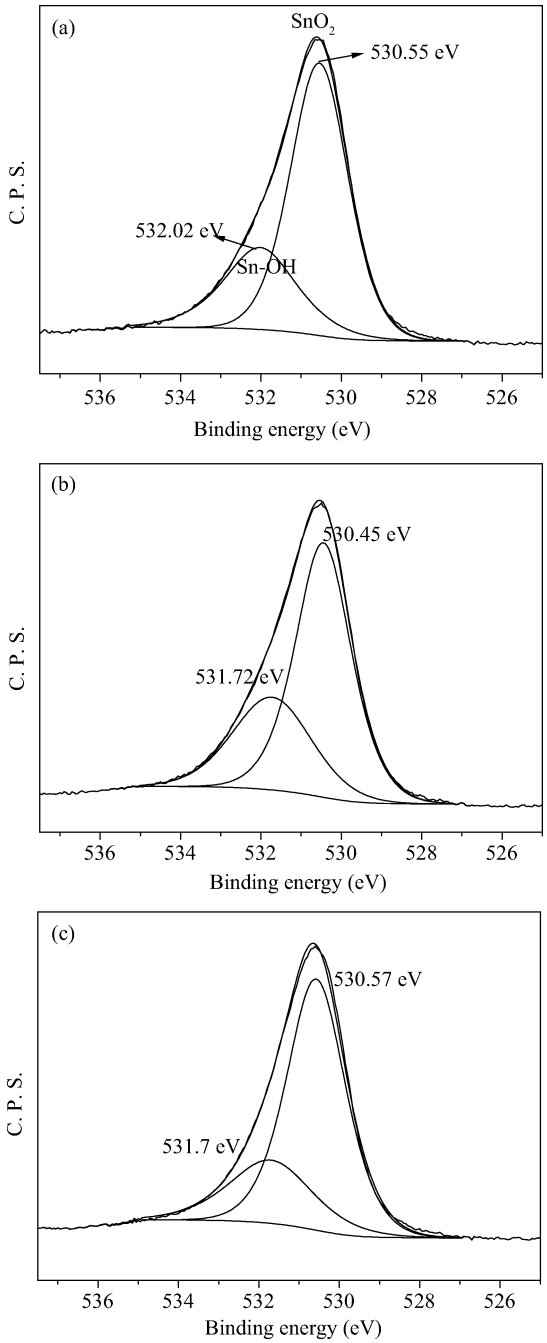

Fig. 9. O1s narrow scan XPS spectra of Sb:SnO_2 thin films deposited for various quantities of spraying solution. (a) 20 cc. (b) 30 cc. (c) 40 cc.

which confirms that the sample deposited with 20 cc solution quantity is oxygen deficient.

3.4. Optical properties

Figure 10 shows the spectral transmittance as a function of wavelength for Sb:SnO_2 thin films deposited with a solution quantity between 20 to 40 cc at a fixed substrate temperature of $T_s = 475$ ℃. It is seen that transmittance decreases with increasing solution quantity. The low transmittance is attributed to increasing thickness, which causes surface darkening. At higher (30, 40 cc) solution quantities, it consists of more Sn^{4+} ions; therefore, films prepared with this solution

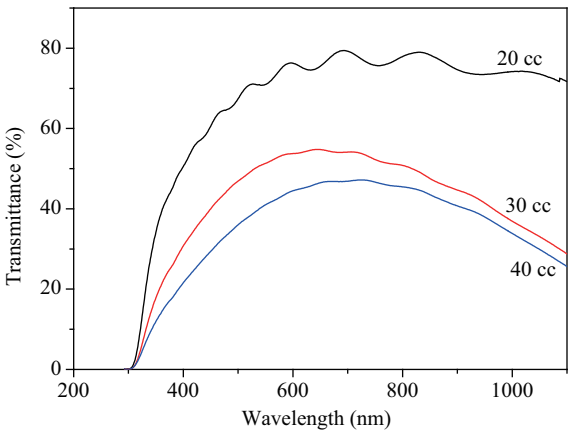

Fig. 10. Variation of transmittance with wavelength for Sb:SnO_2 thin films deposited for various quantities of spraying solution.

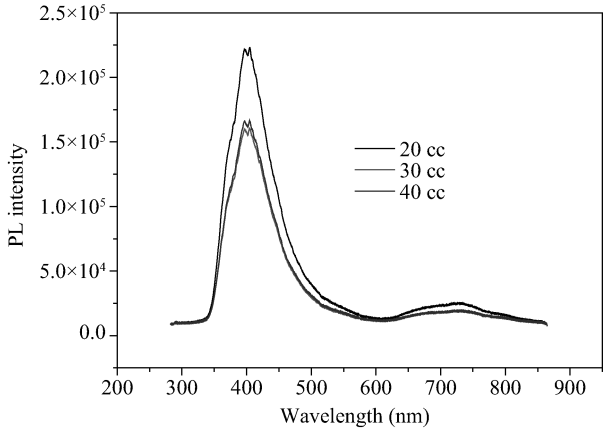

Fig. 11. PL emission spectra of Sb:SnO_2 thin films for various quantities of spraying solution.

are thicker and consequently less transparent. At higher thickness, the films tend to be powdery in nature and whitish in appearance. However, there is a slight shift in the absorption band edge. The shift in the absorption edge can be accounted for by the increase in carrier concentration and blocking of low energy transitions[34]. The transmittance of all of the films decreased with the increasing wavelength. In this case, increasing thickness results in decreasing sheet resistance and increasing carrier concentration ($\approx 10^{20}$ cm^{-3}). The Drude's model is generally used to study the decrease in transmittance in the near infrared region[35]. Briefly, this model indicates that the plasma frequency is proportional to the square root of the carrier concentration.

3.5. Photoluminescence

The room temperature PL emission spectra of Sb:SnO_2 thin films deposited with various solution quantities recorded in the range 350–850 nm is shown in Fig. 11. For all samples, an intensive violet emission peak at 395 nm (about 3.14 eV) and shoulders around 366, 423 and 473 nm (3.39, 2.92 and 2.62 eV) are observed. In addition to this, there is a broad peak at 661 and 718 nm (about 1.88 and 1.73 eV). At room temperature, the high density of oxygen vacancies interacting with

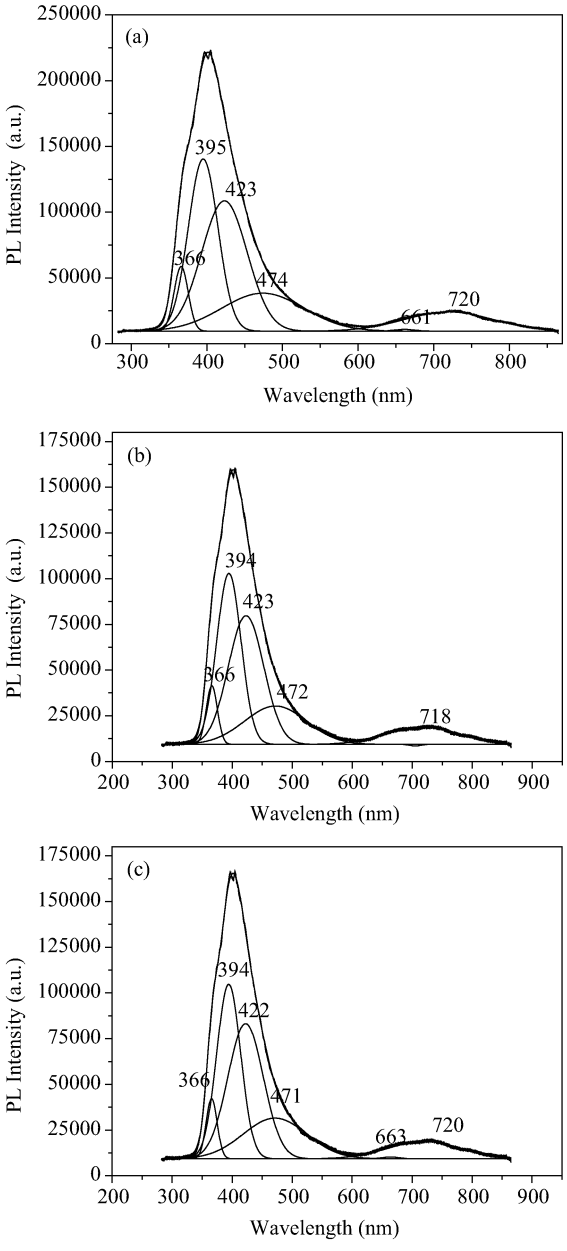

Fig. 12. Gaussian fitted PL spectra of Sb:SnO_2 thin films for various quantities of spraying solution. (a) 20 cc. (b) 30 cc. (c) 40 cc.

interfacial tin leads to the formation of a considerable amount of trapped states within the band gap, giving rise to high PL intensity. Figures 12(a)–12(c) depict the Gaussian profile fitting of the samples deposited using 20, 30 and 40 cc solution quantities. The origin of the peak at 395 nm (3.14 eV) is attributed to the electron transition from the donor level formed by oxygen vacancies (V_O) or Sb^{5+} ions to the acceptor level formed by the Sb^{3+} ions[36]. In spray deposited polycrystalline oxides, oxygen vacancies are known to be the most common defects and form the donor level[37]. For our samples, because of the pyrolytic decomposition, there should be the existence of oxygen vacancies due to rapid evaporation and oxidation processes. The basis of peak at 424 nm can be ascribed to the luminescence centres formed by tin interstitials (S_{ni}) or dangling bonds present in the SnO_2 thin films[38]. Another peak appeared at 474 nm, which corresponds to blue luminescence and can be attributed to singly charged oxygen vacancies (V_O) or luminescent centres in the films[39]. The orange emission observed at 661 nm might be due to the involvement of interstitial oxygen (O_i) ions or due to recombinations from the conduction band and shallow donor levels to the energy levels near the top of the valence band[40]. A broad peak observed at 718 nm for all films may be due to other crystal defects which are formed during the growth of samples. Figures 12(a)–12(c) indicate the various emissions observed in Sb:SnO_2 thin films with various solution quantities. It is seen that there is slight shifting in the emission lines due to variation in solution quantities. Sn_i, O_i and V_O dominate in the defect structure of SnO_2 due to the multi-valence of tin, explaining the natural non-stoichiometry of this material[41]. From Fig. 11, it is seen that the intensity of the violet peak is at a maximum for a 20 cc solution quantity and thereafter decreases. At 20 cc spraying solution, the oxygen vacancies are more, which leads to an increase in the intensity of the violet emission which is confirmed by XPS.

3.6. Electrical properties

Analysis of the electrical properties of Sb:SnO_2 thin films deposited with various solution quantities is carried out using the Van der Pauw technique[42]. The values of electrical resistivity along with other parameters are tabulated in Table 1. Both the sheet resistance and the resistivity are found to decrease with increasing quantity of spraying solution. This resistivity behaviour is due to the increase in the regular sites of the Sn atoms in the films network. Consequently, Sn^{4+} ions are more concentrated in films prepared with a higher quantity regarding the oxygen ions, which results in an increase in the free electron concentration; thereafter there is a decrease in the film's resistivity[17]. The Hall effect measurement confirms that the films exhibit n-type conductivity.

Table 1 also depicts the carrier concentration (n) and carrier mobility (μ) of the Sb:SnO_2 thin film for different solution quantities. The carrier concentration for the film deposited with a 20 cc solution quantity is 5.19×10^{20} cm^{-3} and increases further for higher solution quantities. The maximum carrier concentration of 8.52×10^{20} cm^{-3} is observed for the films deposited with a 40 cc quantity. With increasing solution quantity, the Hall mobility decreased from 9.83 to 7.49 $cm^2/(V{\cdot}s)$. The decrease in mobility with increasing solution quantity is due to increasing conductivity and carrier concentration.

The mean free path (l) is calculated by using the following relation,

$$l = \frac{h}{2e}\left(\frac{3n}{\pi}\right)^{1/3}\mu, \tag{4}$$

where h is Plank's constant, e the electron charge, n the carrier concentration and μ the Hall mobility. The mean free path decreases with increasing quantity of spraying solution (Table 1). The mean free path for Sb:SnO_2 thin films deposited with 20, 30, 40 cc solution quantities is 16.07, 15.56, 14.44 Å, respectively. Since the l values are considerably shorter than the grain size (as seen in FE-SEM images), the Hall mobility is limited by the ionized impurity scattering rather than the grain boundary scattering.

The film degeneracy is confirmed by evaluating the Fermi

energy using the relation

$$\Delta E = \left(\frac{h^2}{8m^*}\right)\left(\frac{3n}{\pi}\right)^{2/3}. \quad (5)$$

The value of the effective mass ($m^* = 0.19m_e$) is evaluated from the plasma frequency for antimony doped SnO_2 films. The calculated value of the Fermi energy lies in the range of 1.24–1.72 eV (Table 1). Fermi energy values of Sb:SnO_2 films are higher compared to kT at room temperature, which is evidence for the degenerate nature of the materials.

For optoelectronic device applications, the figure of merit (ϕ) plays an important role. The device performance is determined from ϕ and is calculated by using the formula[43],

$$\phi = \frac{T^{10}}{R_{Sh}}, \quad (6)$$

where T the transmittance at 550 nm and R_{Sh} is the sheet resistance.

The sheet resistance R_{Sh} is a main factor for the figure of merit, which is calculated by the Van der Pauw technique. The variation in the figure of merit with solution quantity is shown in Table 1. The figure of merit decreases with respect to solution quantity. The obtained highest figure of merit is about $2.11 \times 10^{-3}\ \Omega^{-1}$ for the film deposited with a 20 cc solution quantity.

4. Conclusions

The growth kinetics and physical properties of Sb:SnO_2 thin films with the quantity of spraying solution have been successfully investigated by spray pyrolysis. These films are polycrystalline in nature, highly textured and have a tetragonal crystal structure with (211) and (112) reflections. The big and faceting polyhedron like nanocrystals are observed in the FE-SEM images. The analysis of core levels of the prepared films has been undertaken with the help of X-ray photoelectron spectroscopy. Strong violet emission has been seen in the luminescence spectra. The highest figure of merit is achieved at about $2.11 \times 10^{-3}\ \Omega^{-1}$ at a 20 cc quantity of solution. These films are highly applicable to short wavelength optoelectronic devices and gas sensors.

Acknowledgement

One of the authors (A. R. Babar) is highly grateful to the University Grants Commission, New Delhi, for its support through a UGC meritorious fellowship.

References

[1] Vaufrey D, Khalifa M B, Besland M P, et al. Reactive ion etching of sol–gel-processed transparent conductive oxide as a new material for organic light emitting diodes. Synthetic Metals, 2002, 127: 207

[2] El-Etre A Y, Reda S M. Characterization of nanocrystalline SnO_2 thin film fabricated by electrodeposition method for dye-sensitized solar cell application. Appl Surf Sci, 2010, 256: 6601

[3] Chappel S, Zaba A. Nanoporous SnO_2 electrodes for dye-sensitized solar cells: improved cell performance by the synthesis of 18 nm SnO_2 colloids. Sol Energ Mat Sol Cells, 2002, 71: 141

[4] Vilaseca M, Coronas J, Cirera A, et al. Development and application of micromachined Pd/SnO_2 gas sensors with zeolite coatings. Sensors and Actuators B: Chem, 2008, 133: 435

[5] Fang C, Wang S, Wang Q, et al. Coralloid SnO_2 with hierarchical structure and their application as recoverable gas sensors for the detection of benzaldehyde/acetone. Mater Chem Phys, 2010, 122: 30

[6] Jin J, Seong-Pyung C, Ik C C, et al. Photoluminescence properties of SnO_2 thin films grown by thermal CVD. Solid State Commun, 2003, 127: 595

[7] Kim T W, Lee D U, Yoon Y S. Microstructural, electrical and optical properties of SnO_2 nanocrystalline thin films grown on InP (100) substrates for applications as gas sensor devices. J Appl Phys, 2000, 88: 3759

[8] Gu F, Wang S F, Song C F, et al. Synthesis and luminescence properties of SnO_2 nanoparticles. Chem Phys Lett, 2003, 372: 451

[9] Montero J, Herrero J, Guillén C. Preparation of reactively sputtered Sb-doped SnO_2 thin films: Structural, electrical and optical properties. Sol Energy Mat Sol Cells, 2010, 94: 612

[10] Kane J, Schweizer H P, Kern W. Chemical vapor deposition of antimony-doped tin oxide films formed from dibutyl tin diacetate. J Electrochem Soc, 1976, 123: 270

[11] Carlson D E. The deposition of tin oxide films from a D-C glow discharge. J Electrochem Soc, 1975, 122: 1334

[12] Orel B, Štankgar U L, Crnjak-Orel Z, et al. Structural and FTIR spectroscopic studies of gel-xerogel-oxide transitions of SnO_2 and SnO_2:Sb powders and dip-coated films prepared via inorganic sol–gel route. J Non-Cryst Solids, 1994, 167: 272

[13] Seo M, Akutsu Y, Kagemoto H. Preparation and properties of Sb-doped SnO_2/metal substrates by sol–gel and dip coating. Ceramics International, 2007, 33: 625

[14] Rajpure K Y, Kusumade M N, Neumann-Spallart M N, et al. Effect of Sb doping on properties of conductive spray deposited SnO_2 thin films. Mater Chem Phys, 2000, 64: 184

[15] Thomas B, Benoy S, Radha K K. Influence of Cs doping in spray deposited SnO_2 thin films for LPG sensors. Sensors and Actuators B: Chem, 2008, 133: 404

[16] Rozati S M. The effect of substrate temperature on the structure of tin oxide thin films obtained by spray pyrolysis method. Mater Charact, 2006, 57: 150

[17] Kaneko H, Miyame K. Physical properties of antimony-doped tin oxide thick films. J Appl Phys, 1982, 53: 3629

[18] Ma H L, Hao X T, Ma J, et al. Thickness dependence of properties of SnO_2:Sb films deposited on flexible substrates. Appl Surf Sci, 2002, 191: 313

[19] Agashe C, Mahamuni S. Competitive effects of film thickness and growth rate in spray pyrolytically deposited fluorine-doped tin dioxide films. Thin Solid Films, 2010, 518: 4868

[20] Yannopoulos L N. A p-type semiconductor thick film gas sensor. Sensors and Actuators, 1987, 12: 77

[21] Babar A R, Shinde S S, Moholkar A V, et al. Structural and optoelectronic properties of antimony incorporated tin oxide thin films. J Alloy Compd, 2010, 505: 416

[22] Major S, Banerjee A, Chopra K L, et al. Thickness-dependent properties of indium-doped ZnO films. Thin Solid Films, 1986, 143: 19

[23] Shinde S S, Shinde P S, Bhosale C H, et al. Optoelectronic properties of sprayed transparent and conducting indium doped zinc oxide thin films. J Phys D: Appl Phys, 2008, 41: 105109

[24] Kim D, Kim S. AFM observation of ITO thin films deposited on polycarbonate substrates by sputter type negative metal ion source. Surf Coat Technol, 2003, 176: 23

[25] Phani A R. X-ray photoelectron spectroscopy studies on Pd

doped SnO_2 liquid petroleum gas sensor. Appl Phys Lett, 1997, 71: 2358
[26] Rao L K, Vinni V. Novel mechanism for high speed growth of transparent and conducting tin oxide thin films by spray pyrolysis. Appl Phys Lett, 1993, 63: 608
[27] Terrier C, Chatelon J P, Roger J A. Analysis of antimony doping in tin oxide thin films obtained by the sol–gel method. J Sol–Gel Sci Tech, 1997, 10: 75
[28] Kong J, Deng H, Yanga P, et al. Synthesis and properties of pure and antimony-doped tin dioxide thin films fabricated by sol–gel technique on silicon wafer. Mater Chem Phys, 2009, 114: 854
[29] Bonnelle J P, Grimblot J, D'huysser A. Influence de la polarisation des liaisons sur les spectres esca des oxydes de cobalt. J Electron Spectrosc Relat Phenom, 1975, 7: 151
[30] Ghuang T J, Brundle C R, Rice D W. Interpretation of the X-ray photoemission spectra of cobalt oxides and cobalt oxide surfaces. Surf Sci, 1976, 59: 413
[31] Sharma D D, Hegde M S, Rao C N R. Study of surface oxidation of rare-earth metals by photoelectron spectroscopy. J Chem Soc Faraday Trans II, 1981, 77: 1509
[32] Mulla I S, Rao V J, Soni H S, et al. Electron spectroscopic studies on films of SnO_2 and SnO_2:Sb. Surf Coat Technol, 1987, 31:77
[33] Krishnakumar T, Jayaprakash R, Pinna N, et al. Structural, optical and electrical characterization of antimony–substituted tin oxide nanoparticles. J Phys Chem Solids, 2009, 70: 993
[34] Girtan M, Rusu G I, Gurlui S. Influence of oxidation conditions on the properties of indium oxide thin films. Appl Surf Sci, 2000, 162: 492
[35] Lee S Y, Park B O. Structural, electrical and optical characteristics of SnO_2:Sb thin films by ultrasonic spray pyrolysis. Thin Solid Films, 2006, 510: 154
[36] Shinde S S, Shinde P S, Sathe V G, et al. Electron–phonon interaction and size effect study in catalyst based zinc oxide thin films. J Mol Struc, 2010, 984: 186
[37] Babar A R, Shinde S S, Moholkar A V, et al. Sensing properties of sprayed antimony doped tin oxide thin films: solution molarity. J Alloys Compd, 2011, 509: 3108
[38] Calestani D, Lazzarini L, Salviati G, et al. Morphological, structural and optical study of quasi-1D SnO_2 nanowires and nanobelts. Cryst Res Technol, 2005, 40: 937
[39] Rani S, Roy S C, Karar N, et al. Structure, microstructure and photoluminescence properties of Fe doped SnO_2 thin films. Solid State Commun, 2007, 141: 214
[40] Zhang D, Guo D, Pu X, et al. Rapid synthesis of ZnO ellipsoidal nanostructures in large scale and their photoluminescence properties. Mater Lett, 2009, 63: 2290
[41] Kilic C, Zunger A. Origins of Coexistence of conductivity and transparency in SnO_2. Phys Rev Lett, 2002, 88: 095501
[42] Shinde S S, Shinde P S, Pawar S M, et al. Physical properties of transparent and conducting sprayed fluorine doped zinc oxide thin films. Solid State Sciences, 2008, 10: 1209
[43] Babar A R, Deshamukh P R, Deokate R J, et al. Gallium doping in transparent conductive ZnO thin films prepared by chemical spray pyrolysis. J Phys D: Appl Phys, 2008, 41: 135404